A glass neutron detector with machine learning capabilities

Published by IOP Publishing for Sissa Medialab

Received: *March 8, 2019*
Revised: *May 2, 2019*
Accepted: *May 23, 2019*
Published: *June 11, 2019*

2019 JINST 14 P06013

A glass neutron detector with machine learning capabilities

G.L. Ademoski,[a,1] **S. Simko,**[a,1] **M. Teeple,**[a,1] **I. Morrow,**[a,1] **P. Kralik,**[a] **C.J. Wilkinson,**[a,b] **G. Varney,**[a] **M. Martinez-Szewczyk,**[a] **L. Yinong,**[c] **J.K. Nimmagadda,**[d] **S. Samant,**[e] **Y. Wu,**[f] **L. Pan,**[f] **L.G. Jacobsohn,**[f] **Q. Wilkinson,**[a] **F. Duru**[a] **and U. Akgun**[a,2]

[a] *Physics Department, Coe College, Cedar Rapids, IA 52402, U.S.A.*
[b] *Department of Materials Science and Engineering, The Pennsylvania State University, University Park, PA 16802, U.S.A.*
[c] *Department of Nuclear and Radiological Engineering, University of Florida, Gainesville, FL 32610, U.S.A.*
[d] *Department of Materials Science and Engineering, University of Florida, Gainesville, FL 32610, U.S.A.*
[e] *Department of Radiation Oncology, University of Florida College of Medicine, Gainesville, FL 32610, U.S.A.*
[f] *Department of Materials Science and Engineering, Clemson University, Clemson, SC 29634, U.S.A.*

E-mail: uakgun@coe.edu

[1] These authors contributed equally to this work.
[2] Corresponding author.

https://doi.org/10.1088/1748-0221/14/06/P06013

Abstract: The detection of neutrons above background levels is an indication of nuclear materials, creating significant applications for handheld neutron detectors in homeland security. For such applications, a ^{10}B and ^{6}Li enriched, scintillating glass neutron detector was designed. The model is compact enough to be used as a handheld detector and is equipped with machine learning capabilities to determine the location of the source and discriminate a neutron from a gamma. Lithium Borosilicate glass samples, with up to 70% ^{10}B and ^{6}Li content, and doped with Tb and Eu, were engineered to optimize the performance of the detector. The scintillation properties and neutron/gamma detection capabilities of the glass samples were tested. The model detector's performance was simulated in Geant4 and the simulation data was utilized for machine learning to predict the location of the source with an Artificial Neural Network (ANN). The reported handheld neutron detector design with the implemented artificial intelligence capability can achieve 99.9% accuracy in neutron/gamma discrimination, 8.9% error in radial angle estimates, and 2.9% error in azimuthal angle estimates.

Keywords: Detector modelling and simulations I (interaction of radiation with matter, interaction of photons with matter, interaction of hadrons with matter, etc); Neutron detectors (cold, thermal, fast neutrons); Scintillators, scintillation and light emission processes (solid, gas and liquid scintillators)

2019 JINST 14 P06013

Contents

1 Introduction

The neutron's neutral charge makes it very difficult to detect [1–10]. Most current neutron detectors rely on expensive isotopes such as ^{3}He or ^{6}Li. ^{10}B offers an alternative material for neutron detection through the following mechanisms [10]:

$$^{10}\mathrm{B} + \mathrm{n} \rightarrow {}^{7}\mathrm{Li} + \alpha(1.78\,\mathrm{MeV}) - 6\%\ \text{probability}$$
$$^{10}\mathrm{B} + \mathrm{n} \rightarrow {}^{7}\mathrm{Li} + \alpha(1.47\,\mathrm{MeV}) + \mathrm{gamma}(0.48\,\mathrm{MeV}) - 94\%\ \text{probability}$$

In the thermal energy region, the ^{10}B cross section for neutron capture increases up to ~4000 barns. The ^{10}B enriched scintillating glasses are easy to make, cost effective, and allow more freedom in the design geometry of the detector [3–6]. The alpha and gamma particles generated from the neutron capture process yield enough photons in a ^{10}B enriched scintillating glass for detection [7].

^{10}B-based glass scintillators were first studied with a focus on glasses containing Boron, Sodium, Aluminum, and Cerium as the scintillator [3]. In a separate study, it was also shown that glasses increase their neutron capturing efficiency with higher Boron concentration [4]. This shows that Cerium-doped Borosilicate glasses, even with natural Boron, can be effectively used for neutron detection [3, 4]. This also allows for the potential usage of other high efficiency scintillators such as Terbium and Europium [11].

Since these initial results, many of the following studies in the area have focused on ^{6}Li as the neutron-capture mechanism due to the significant α-particle peak in ^{10}B events. However, in the thermal energy region, the neutron-capturing cross-section of ^{10}B is over four times larger than that of ^{6}Li, which makes ^{10}B glasses a crucial candidate. ^{10}B glasses are also verified to have a significantly shorter decay time than similar ^{6}Li glasses [6]. However, increasing the ^{10}B concentration within the glass, beyond a certain percentage, has been shown to reduce the scintillating light production [7].

In this study in order to maximize the neutron capturing ability, a lithium borosilicate glass sample with ^{6}Li and ^{10}B is reported. This combination uses the ability of ^{6}Li to capture neutrons via,

$$^{6}\mathrm{Li} + \mathrm{n} \rightarrow {}^{3}\mathrm{H} + \alpha(2.05\,\mathrm{MeV})$$

2019 JINST 14 P06013

This way up to 70% of the active media within the scintillating glass has neutron capturing capabilities. Terbium and Europium are preferred as scintillating agents, due to their higher light yields compared to Cerium.

Most current neutron detectors can reliably detect neutron radiation. However, modern security needs demand more features, in particular the tracking information. Binary information is available in most modern detectors but they are typically orientation-sensitive [10]. Designs with layered bar architectures have also been shown to be effective methods for the detection and track reconstruction of charged particles [11]. In this particular case, due to the few secondary particles that also remain highly localized within the detector traditional track, reconstruction is relatively difficult. In order to accurately reconstruct the location of the source, machine learning is deployed. Machine learning (ML) has become widely used due to its ability to estimate unknown functions [12–15]. Though ML has many associated techniques, in this report, neural networks are the main focus due to their ability to approximate a function based solely on input and output data.

Herein a scintillating glass based handheld neutron detector design with machine learning capabilities is summarized. The following sections give detailed descriptions of the glass making conditions, testing of the optical properties, and testing of the neutron capturing abilities of these glasses. The report also summarizes the Geant4 [16, 17] simulations performed on the layered bar architecture [11] and the machine learning studies based on this unique detector design.

2 Results

2.1 Developing the boron-10 enriched glass

In the study described here, a Lithium Borosilicate glass, with concentrations $30Li_2CO_3$-$30SiO_2$-$40B_2O_3$, was used as its properties are well established, generates a glass matrix near the peak of Q^4 units (to optimize stability and density [18]), and results in a transparent glass sample. In comparison to a soda-lime ^{10}B scintillating glass reported earlier [9], this glass has potential to contain up to 7 times as much neutron capturing Lithium and Boron components. Silica is used to increase stability and thus durability of the glass due to the connectivity increase.

The glass samples were produced with base composition of 30% Li_2CO_3, 30%SiO_2, and 40% B_2O_3 (molar %) and up to 7% scintillating agents of Tb_4O_7 or Eu_2O_3. All glasses produced were enriched with ^{10}B, and one 4% Tb-doped sample was enriched with ^6Li (to compare relative activity). The sample containing ^6Li had a final composition of $30Li_2CO_3$-$30SiO_2$-$40B_2O_3$-4Tb (molar %), and all of the chemicals were of at least 99.9% purity. The components were individually weighed in a platinum crucible, zeroing the scale after each component was added. Chemicals were added in order of least to most contribution to the total mass. After all the components were added, the powder was mixed for ten minutes. The crucible was heated in a furnace for 30 minutes at 1250°C. The crucible was then removed and weighed to check for errors in the experimental weight loss and then placed back into the furnace for an additional 10 minutes for a final melt. The glass was then poured onto a preheated steel mold at 500°C and annealed for 1 hour at this temperature. The resulting sample had no cracks and high transparency with cutoff wavelength at 340 nm.

Photoluminescence (PL) measurements were executed with an Edinburgh Instruments FLS-1000 spectroflurometer equipped with a 450 W Xe lamp and dual monochromators for the excitation,

2019 JINST 14 P06013

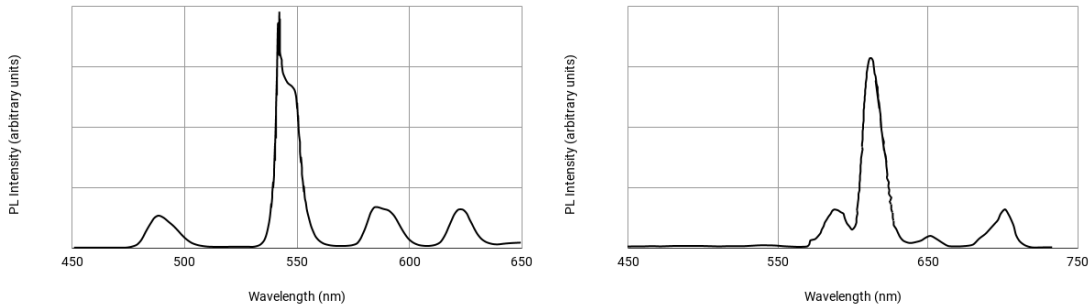

Figure 1. Photoluminescence measurement of the glass sample with composition $30Li_2CO_3$-$30SiO_2$-$40B_2O_3$-4Tb [Left] and $30Li_2CO_3$-$30SiO_2$-$40B_2O_3$-6Eu [Right].

set at 245 nm, and the emission, within 350 and 650 nm. The absolute fluorescence quantum yield for the total integrated emission within 450 nm and 750 nm was determined using a 120-mm diameter integrating sphere under 350 nm excitation.

PL spectra of Tb doped glasses were dominated by an emission band peaking at 542 nm with three additional weak bands (see figure 1 Left). These bands were assigned to the 5D4 → 7FJ, with J = 6, 5, 4, and 3, of Tb^{3+} ions for increasing wavelengths respectively. The 5D3 → 7FJ transitions within 350–450 nm were not observed. The absolute quantum yield for the total integrated emission within 450 nm and 650 nm was determined to be 30%. The PL spectrum of the Eu doped scintillating glass is very similar to our previous report [11]; weak emission bands at 591 nm, 653 nm, and 700 nm, were observed, with peak emission at 612 nm (see figure 1 Right). The PL measurements showed that 6% Eu and 4% Tb doped glasses yield more scintillation light than the other samples, hence these samples were taken to the beam tests.

2.2 Neutron and gamma tests

The neutron and gamma beam tests were conducted at the University of Florida Test Reactor (UFTR). This reactor is a 100 kW modified argonaut-type reactor moderated with light water and graphite. This allows for low flux and long exposure testing in addition to fine flux adjustments. The samples attached on a PMT window, were wrapped with aluminum foil and electrical tape which created a light tight seal. Scintillation of the sample was measured using a 1 inch diameter Hamamatsu H10580-100 PMT at 10^6 gain. The spectral response range of the PMT is 300 nm–650 nm, which fits well with the PL spectra of the glass samples. The reactor was operated at 10 W for the test beam. At this power, the reactor provides thermal neutrons (energy < 0.025 eV) with a flux of 1.63×10^3 $cm^{-2}s^{-1}$, and epithermal neutrons (energy > 0.025 eV) with a flux of 8.68×10^2 $cm^{-2}s^{-1}$. The gamma radiation the samples were exposed to was measured as 21 mREM/hr, with around 90% of the arriving particles found to be gamma by the UFTR.

The ^{10}B and ^{6}Li enriched scintillating glass samples were coupled to the front window of the PMT with optical coupler. The glass samples (1 cm in diameter), and the front window of the PMT faced the reactor beam ($2'' \times 2''$ dimensions). The same PMT was used for all three glass samples for comparison purposes. A 16 channel DAQ system by Struck Innovative Systeme (model SIS3316-DT, a VME digitizer card) was used for data acquisition. This DAQ system has

2019 JINST 14 P06013

14-bit resolution and 250 a MHz sampling rate, keeping the signal as a Moving Average Window (MAW). Then a moving average (MA) was performed over the programmable peaking time, and then delayed by adding the peaking time and gap time together. This value is used for the trigger threshold algorithm. A threshold of 1 mV was used during the offline analysis performed with Matlab™ [20].

The samples were tested with this mixed gamma and neutron beam coming from the UFTR. In order to discriminate the glass samples' responses to gammas and neutrons, separate runs were taken with a 2″ thick lead shield to block gamma radiation, and a 2 mm thick Cadmium shield to block neutrons. On each run, 15,000 events were recorded. The amount of charge collected by each trigger was used for discrimination purposes since the scintillating light production for a gamma traversing the glass is expected to be different than that of a neutron event. Figure 2 shows the histograms of the Cadmium shield runs (more gamma) subtracted from the Lead shield runs (more neutron) for all three glass samples tested. The negative values on figure 2 are labeled as gamma, and positive bins are labeled as neutron events. On each histogram, one can see the transition between the gamma and neutron events at around the 40–50 pC range (see figure 2). This effect is very obvious in Tb doped glasses (figure 2 Left and Middle), however the Eu doped glass is much weaker in terms of gamma/neutron discrimination.

The glass "Sample-1" with composition $0.3Li^{7}$-$0.4B_2^{10}O_3$-$0.3SiO_2$: 0.04Tb (see figure 2 Left) on average yielded 25.6 pC charge per gamma, and 53.5 pC charge per neutron event. The positive bins in figure 2 Left shows that the Sample-1 detected 629 neutron events out of 15000 triggers, which corresponds to less than half of the neutrons (~10%) reported to be provided by the incoming beam.

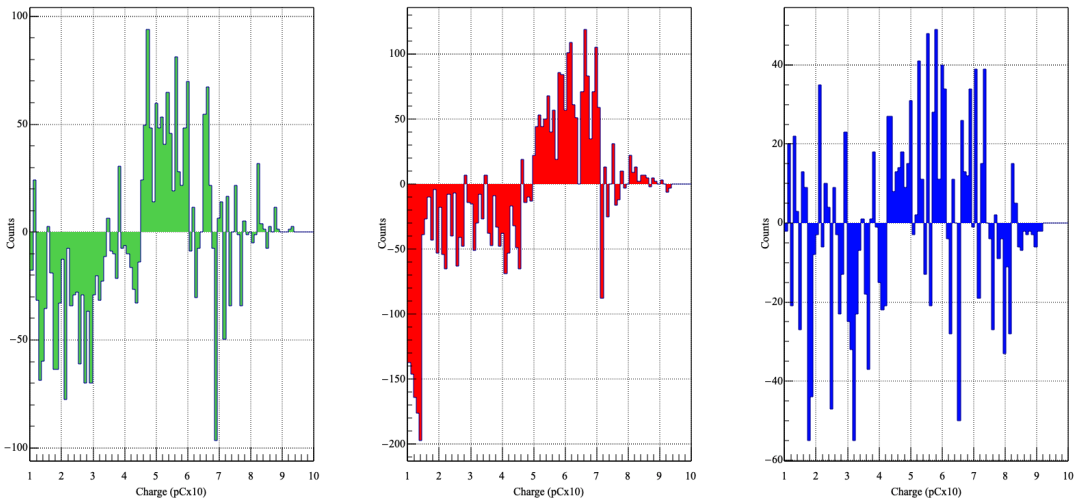

Figure 2. The histograms of the Cadmium shield runs (more gamma) subtracted from the Lead shield runs (more neutron) for three glass samples: $0.3Li^{7}$-$0.4B_2^{10}O_3$-$0.3SiO_2$: 0.04Tb [Left], $0.3Li^{6}$-$0.4B_2^{10}O_3$-$0.3SiO_2$: 0.04Tb [Middle], and $0.3Li^{7}$-$0.4B_2^{10}O_3$-$0.3SiO_2$: 0.06Eu [Right].

2019 JINST 14 P06013

On the other hand, the glass "Sample-2" with composition $0.3Li^{6}$-$0.4B_2^{10}O_3$-$0.3SiO_2$:0.04Tb (see figure 2 Middle), while yielding very similar scintillation light for gamma events (24.5 pC), produced the biggest average signal for neutron events (62.2 pC). The figure 2 Middle histogram gives 1463 neutron events, which corresponds to the 97.5% of the possible neutrons provided by the beam. Since the Sample-2 has two components that can capture neutrons, both ^{10}B and ^{6}Li, not only is the overall average neutron signal bigger, it also clearly captures more neutrons compared to other samples.

The Eu doped scintillating glass "Sample-3" with composition $0.3Li^{7}$-$0.4B_2^{10}O_3$-$0.3SiO_2$:0.06Eu, contains the same amount of ^{10}B as Sample-1, but replaces 4%Tb with 6% Eu doping, which changes the response of the glass drastically. This sample yielded on average 31.3 pC per gamma event and 47.5 pC per neutron event. However, the main difference is in the number of events that can be discriminated as neutrons; the Sample-3 yielded only 349 such triggers out of 15,000. That corresponds to 23% of the possible neutrons provided by the beam.

2.3 Detector simulation and machine learning implementation

The detector performance simulations and the data used for machine learning were generated via Geant4 [16, 17]. The modeled geometry of the detector consisted of ten alternating layers of ten adjacent bars each. The bars were 1 cm × 1 cm × 10 cm, and each was wrapped in 90% reflective material to isolate its signal from that of the others (see figure 3). This resulted in an overall detector size of just around 10 cm × 10 cm × 10 cm, composed of 100 bars of the previously described base glass with composition $0.3Li^{7}$-$0.4B_2^{10}O_3$-$0.3SiO_2$. Each glass bar was wrapped in a thin 1 mm layer of polyethylene to thermalize the incoming neutrons. This geometry was inspired by that of a proton imager detector also designed by the authors of this study [11]. The Geant4 simulations of the prototype detector shows that the number of neutrons captured increases drastically as the neutrons are slowed down (see figure 4). Figure 5 shows the energy distributions of secondary particles from the simulated neutron capturing events of ^{10}B. The theoretical values of alpha energies are 1.78 MeV (6% of the time) and 1.47 MeV (94% of the time), and can clearly be observed in the simulated alpha particle energy distribution (see figure 5 Left). Meanwhile, the produced gamma energy distribution yields a peak at 0.48 MeV as expected (figure 5 Right).

In Geant4 simulations, the detector was located at the origin and a neutron gun fired a beam of neutrons at the center of the detector from randomized spherical coordinates, covering the full solid angle around the detector, with the radial component varying from 100 cm to 17,000 cm. At each incident location, the energy deposited in each of the glass bars was recorded. This series of energy deposition for 100 bars was used as the data to train the AI. All neutrons had an initial energy of 2.5 MeV, which is the average initial energy of neutrons emitted from a radioactive source and the 2.5 MeV gamma particles were also simulated in the same manner. All the Geant4 simulations were performed via 128-core Linux cluster.

A classifier neural network (NN) was used to differentiate between gamma particles and neutrons, while a function approximation NN was used to predict the φ and θ directions of incident neutrons with respect to the detector. Artificial Neural Networks (ANN) were built in Matlab [19] and in Python in conjunction with Keras [14] and TensorFlow [12]. The latter method provided better accuracy. All training was conducted on a gpu GeForce® TURBO-GTX1080TI-11G. For

2019 JINST 14 P06013

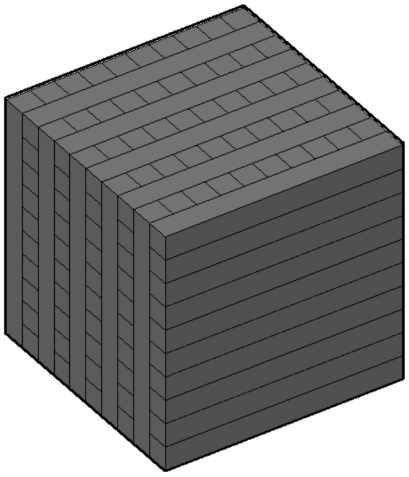

Figure 3. The simulated geometry of the detector design. The neutron capturing B-10 and Li-6 enriched, Tb doped, 100 scintillating glass bars (each with 1 cm × 1 cm × 10 cm dimensions) are stacked in alternating orientations.

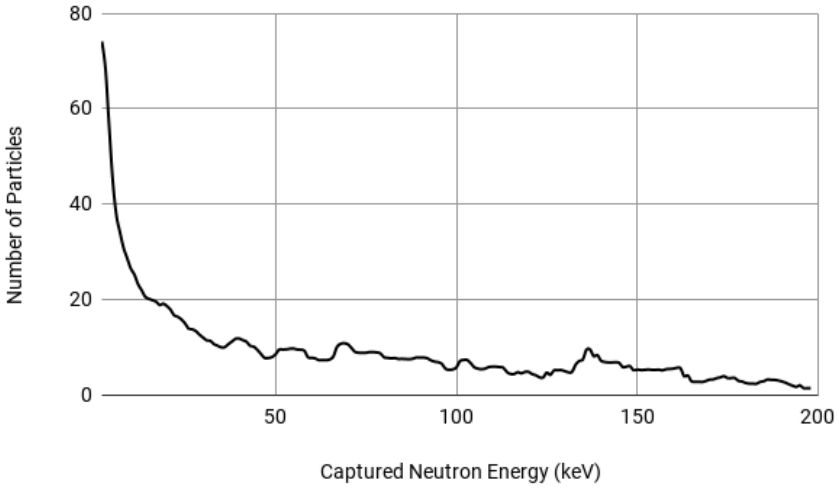

Figure 4. Geant4 simulations on our prototype detector show that the number of neutrons captured increases drastically as the neutrons are slowed down.

both the classifier and function approximation networks, 70% of the generated data was used for training, 15% for validation and 15% for the test of the ANN.

The classifier NN that discriminates between gamma particles and neutrons was trained with 64000 neutrons and 64000 gammas. The pattern of energy deposition on 100 bars for each of the simulated neutron and gamma events was used for machine learning. The ANN with two layers of neurons, fully-connected, 400 neurons on each, were trained with the resilient backpropagation algorithm. After the training, the ANN correctly determines if the incoming particle is a gamma or neutron 99.9% of the time. It is crucial to real world implementation to make sure that gamma particles, which are more prevalent than neutrons, do not give false positives.

2019 JINST 14 P06013

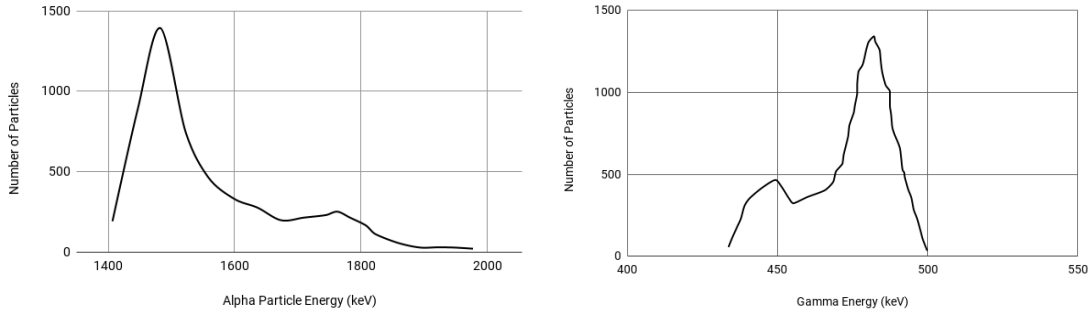

Figure 5. Geant4 simulations on our model yield the alpha particle energy peaks at 1480 keV and 1780 keV [Left]. The gamma energy distribution of our simulations peaks at 480 keV as expected [Right].

The second ANN that is implemented predicts the φ and θ directions of neutrons which are detected. It was trained with 110,000 neutron events. The r, φ and θ coordinates of the neutrons were saved from when they were fired. Initially, the ANN was trained to find the relationship between the known r, φ and θ values and the energy deposited in the detector. However, due to low accuracy in the r dimension, it was dropped. It is believed this low accuracy comes from the low energy deposition in air, so it is hard to discriminate distances from the energies deposited. The remaining dimensions worked well with $\boldsymbol{R^2}$ values of .995 and .992 respectively for the φ and θ values (see figure 6). These plots yield 2.9% error for the azimuthal angle φ and 8.9% error for the radial angle θ. At θ values of 0, 90, 180, 270 and 360 degrees the ANN predicted poorly (see figure 6 Right). This may be because the cubic shaped box is symmetric for the incoming particles at these angles, which fundamentally makes it difficult to predict the path using only the deposition data.

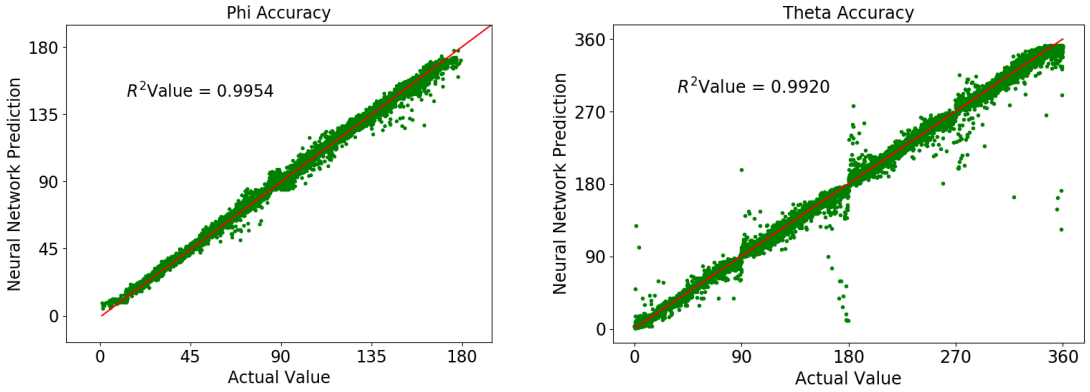

Figure 6. The ANNs predicted values for the φ [Left] and θ [Right] values, plotted against the known values from the Geant4 simulations.

2019 JINST 14 P06013

3 Conclusions

^{10}B and ^{6}Li enriched Terbium/Europium-doped glasses can be used for neutron detectors in many areas, including homeland security. Here, the glass forming conditions for stable, scintillating glass samples with up to 70% neutron capturing contents are outlined. After pursuing high ^{10}B and ^{6}Li concentrations, a relatively high content was achieved for the glass studied.

The final composition's use of ^{10}B rather than natural Boron produced a 42% thermal and epithermal neutron capture rate at 40% B_2O_3concentration, using Tb as a scintillating agent. The same concentration's weaker performance when Eu is used as the scintillating agent, can be explained by: i) Lower PMT spectral sensitivity at the dominant Eu emission band (612 nm) compared to the Tb emission band (512 nm), ii) Eu might be causing structural differences in the glass that creates color centers. When ^{6}Li is used in conjunction with ^{10}B, a stable scintillating glass with 70% neutron capturing ability was successfully produced. This sample performed very well in the test beam with up to 97% thermal/epithermal neutron capturing capability. This composition is also producible in large batches, unlike previous reports [4]. Here, one should keep in mind that during the test beam a borosilicate window PMT was used, and that potentially can contribute some error to these results [20].

Simulated prototype detector performance and geometry optimization studies were performed using Geant4 simulations. The Geant4 simulation results were used to develop a ANN that can discriminate the gamma and neutron signals with 99.9% accuracy. Also, with a separate machine learning training, an AI can predict the azimuthal angle φ and radial angle θ values of the incoming neutrons with 2.9% and 8.9% error, respectively. The r value prediction using the same approach was not as successful with almost 36% error. However, an alternative method for calculation of the r value can be developed based on the detected flux at two different locations and inverse square law.

This study shows that a compact, affordable, handheld scintillating glass neutron detector (see figure 3) with high neutron capturing capabilities is possible. It also shows that the novel geometry of a possible prototype can utilize machine learning techniques to handle large data yields, provide neutron/gamma discrimination capability, and achieve precise directional prediction.

Acknowledgments

This work was supported by NSF-DMR 1407404, NSF-REU 1358968, McElroy Trust, and Coe College. The summarized work also used the material based on work supported by the National Science Foundation under Grant No. 1653016.

References

[1] G.F. Knoll, *Radiation detection and measurements*, John Wiley and Sons, Inc., New York U.S.A. (2000).

[2] A.O. Hanson and J.L. McKibben, *A Neutron Detector Having Uniform Sensitivity from 10 KeV to 3 MeV*, *Phys. Rev.* **72** (1947) 673.

[3] L.M. Bollinger, G.E. Thomas and R.J. Ginther, *Glass scintillators for neutron detection*, *Rev. Sci. Instrum.* **30** (1959) 1135.

2019 JINST 14 P06013

[4] L.M. Bollinger, G.E. Thomas and R.J. Ginther, *Neutron detection with glass scintillators*, *Nucl. Instrum. Meth.* **17** (1962) 97.

[5] T. Kojima et al., *Neutron scintillators with high detection efficiency*, *Nucl. Instrum. Meth.* **A 529** (2004) 325.

[6] M. Ishii et al., *Boron based oxide scintillation glass for neutron detection*, *Nucl. Instrum. Meth.* **A 537** (2005) 282.

[7] A.M. Bishay, *Glass Scintillator for Neutron Detection*, *J. Am. Ceramic Soc.* **44** (1961) 231.

[8] G. Zanella et al., *Development of a Terbium-Lithium Glass for Slow Neutron Detection*, *Nucl. Instrum. Meth.* **A 359** (1995) 547.

[9] D. Vu et al., *A Neutron Detector Based on Boron-10 Enriched Scintillating Glasses*, in *Ceramic Transactions. Vol. 258: Additive Manufacturing and Strategic Technologies* , American Ceramic Society (2016), pg. 59.

[10] R.T. Kouzes and J.H. Ely, *Status summary of 3He and neutron detection alternatives for homeland security*, Technical Report No. PNNL-19360, Pacific Northwest National Laboratory (PNNL), Richland U.S.A. (2010).

[11] C.J. Wilkinson et al., *High density scintillating glass proton imaging detector*, *Proc. SPIE* **10132** (2017) 101323V.

[12] M. Abadi et al., *TensorFlow: A System for Large-Scale Machine Learning*, at *12th USENIX Symposium on Operating Systems Design and Implementation (OSDI 16)*, Savannah U.S.A. (2016), pg. 265 [arXiv:1605.08695].

[13] G.M. Harry for LIGO Scientific collaboration, *Advanced LIGO: the next generation of gravitational wave detectors*, *Class. Quantum Grav.* **27** (2010) 084006.

[14] F. Chollet et al., *Keras*, https://keras.io (2018).

[15] H. Kolanoski, *Application of artificial neural networks in particle physics*, in *International Conference on Artificial Neural Networks*, Skövde Sweden (1998).

[16] S. Agostinelli et al., *Geant4 — a simulation toolkit*, *Nucl. Instrum. Meth.* **A 506** (2003) 250.

[17] J. Allison et al., *Geant4 developments and applications*, *IEEE Trans. Nucl. Sci.* **53** (2006) 270.

[18] M. Shibata et al., *The density of lithium borate glasses related to atomic arrangements*, *J. Non Cryst. Solids* **85** (1986) 29.

[19] MATLAB and Neural Network Toolbox Release R2016b, The MathWorks, Inc., Natick U.S.A..

[20] U. Akgun et al., *Boron and Thermal Neutron Interactions on Borosilica Window Photomultiplier Tubes*, 2010 *JINST* **5** P08005.

2019 JINST 14 P06013